Free vibration analysis of tapered FRP transmission poles with flexible joint by finite element method

Behnam Saboori[*1] and Seyed Mohammad Reza Khalili[1,2a]

[1]Centre of Excellence for Research in Advanced Materials & Structures, Faculty of Mechanical Engineering, K.N. Toosi University of Technology, Pardis St., Molasadra Ave., Vanak Sq., Tehran, Iran
[2]Faculty of Engineering, Kingston University, London, UK

Abstract. Since relatively low elasticity modulus of the FRP materials results in lower natural frequencies, it is necessary to study the free vibration of FRP transmission poles. In this paper, the free vibration of tapered FRP transmission poles with thin-walled circular cross-section is investigated by a tapered beam element. To model the flexible joints of the modular poles, a rotational spring model is used. Modal analysis is performed for typical FRP poles with/without joint and they are also modeled by ANSYS commercial finite element software. There is a good correlation between the results of the tapered beam finite element model and those obtained from ANSYS as well as the existing experimental results. The effects of different geometries, material lay-ups, concentrated masses at the pole tip, and joint flexibilities are evaluated. Moreover, it is concluded that using tougher fibres at the inner and outer layers of the cross-section, results in higher natural frequencies, significantly.

Keywords: transmission pole; fiber-reinforced polymer; flexible joint; free vibration; finite element method

1. Introduction

Traditional materials like wood, concrete and steel are usually used to construct power transmission and distribution poles. Considering the materials restrictions and defects for application in power transmission and distribution lines, there are many motivations for replacing the traditional poles with FRP (fibre-reinforced polymers) ones. The poles are made of polymer matrix with reinforcing fibre, mostly fabricated by filament winding technique. Polyester, vinylester or epoxy is mainly used as a matrix and E-glass, S-glass, aramid or carbon fibres as reinforcement (Yuan *et al.* 1991).

Transmissions poles are mainly subjected to cantilever bending due to wind gusts and cables weight, and mostly are tapered and thin-walled members. Many studies have been performed on the dynamic behavior of thin-walled sections made of steel as well as composite materials, but only a few on tapered sections. In fact, the vast majority of studies are concerned with the dynamic

---

behavior of tapered members made from homogeneous and isotropic materials (Yuan *et al.* 1991, Polyzois *et al.* 1998).

The major weaknesses of FRP poles are high initial cost and low stiffness. Reduction of the initial cost is a long term process and involves multi-disciplinary efforts. The problem associated with lower stiffness, such as excessive deformation and instability, is more technical and must be addressed before any consideration for practical use of FRP poles. Due to the complexity of material properties, layer lay-ups, fibre orientations, tapered shape, and combination of loads of FRP transmission poles, the pure analytical method is incapable of providing acceptable solutions effectively and on the other hand, numerical analysis methods are proved to be more efficient (Lin 1995).

Navaratna *et al.* (1968) are among the early researchers to use the finite element method (FEM) to analyze the stability of the shells of revolution. The approach used by them to develop the geometric stiffness matrix is followed by Gould and Basu (1977) for the linear buckling and the incremental deformation analysis of rotational shells. Finite element method was used by Ibrahim and Polyzois (1999) to analyze the cross-section ovalization behavior of FRP poles under a bending load. Based on their study, circumferential layers tend to increase the critical ovalization load of FRP poles. The coupled stability analysis of thin-walled FRP beams with closed cross-section subjected to various forces such as eccentric constant axial force, end moments, and linearly varying axial force was performed using the Hermitian beam elements by Kim *et al.* (2010). In addition, full-scale static flexural testing on FRP poles was conducted by Metiche and Masmoudi (2007). Mohamed and Masmoudi (2009) presented several finite element simulations of the nonlinear behavior of laterally loaded full scale tapered GFRP poles by a commercial finite element software. The finite element simulations were used to detect the performance of glass fibre-reinforced polymer (GFRP) poles having service opening. Recently, Zabihollah and Ganesan (2010) conducted the buckling analysis of laminated tapered composite beams using a higher order finite element formulation which ensures the continuity of the stress distribution through the thickness of a laminate as well as across the element interfaces.

On the other hand, Mabie and Rogers (1972, 1974) presented a closed-form solution to the free vibration of an isotropic double-tapered cantilever beam with rectangular cross-section and end mass. The beam was tapered linearly in the horizontal and vertical planes simultaneously, with the taper ratio in the horizontal plane equal to that in the vertical plane. Noor *et al.* (1991) assessed a group of computational methods for multilayered composite cylinders. The finite element models they surveyed are mostly two or three-dimensional elements. Caracoglia and Jones (2007) performed a numerical and experimental study of vibration mitigation for highway tapered aluminum poles. The study was performed in order to identify the potential causes associated with the failures. It was concluded that, although the poles were designed according to standard specifications, an unusual event, in which the combination of wind and frozen precipitation was observed, could be responsible for large vibration amplitudes. Caracoglia and Velazquez (2008) also compared the dynamic performance of steel, aluminum and GFRP light poles through experimental testing. The comparison of the performances was based on frequency and damping ratios corresponding to the first and the second-mode vibrations.

The current study deals with the investigation of the free vibration behavior of tapered FRP transmission poles utilizing tapered beam finite element (Polyzois *et al.* 1998) model. In the model, the pole cross-section is considered thin-walled circular and also as a symmetric or anti-symmetric angle-ply laminate and, the shear effects are accounted for, because of their significant role. In

addition, to model the flexible joints of jointed FRP poles, a simple model considering the joint as a rotational spring (Raftoyiannis and Polyzois 2007) is employed. Modal analysis is performed for typical FRP poles with/without joint and they are also modeled by ANSYS version 11.0 commercial finite element software using 3D SHELL99 elements, and to model adhesive joints of the jointed pole, surface-to-surface contact is used. A good correlation between the results of the tapered beam finite element model and those obtained from ANSYS as well as the existing experimental results is demonstrated. Then, through a parametric study the effects of different geometries, material lay-ups, concentrated masses at the pole tip, and the joint flexibilities are evaluated using the tapered beam finite element model. As a solution to increase the FRP poles natural frequencies, use of stiffer fibres at the outer and inner layers of the cross-section is suggested. This suggestion is also investigated and the results are represented in this paper.

2. Effective elasticity modulus

Using the classical lamination theory, the stiffness components of each generally orthotropic lamina can be determined and the constitutive equation for the laminate is (Jones 1998)

$$\left\{ \begin{array}{c} \mathbf{N} \\ \mathbf{M} \end{array} \right\} = \left[\begin{array}{cc} \mathbf{A} & \mathbf{B} \\ \mathbf{B} & \mathbf{D} \end{array} \right] \left\{ \begin{array}{c} \boldsymbol{\varepsilon} \\ \boldsymbol{\kappa} \end{array} \right\} \tag{1}$$

where $\mathbf{N}$ and $\mathbf{M}$ are the stress resultants and stress couples, respectively. $\boldsymbol{\varepsilon}$ and $\boldsymbol{\kappa}$ are the strains and the curvatures. The stiffness coefficients A_{ij}, B_{ij}, and D_{ij} correspond to extensional, coupling, and bending stiffness coefficient and are defined as follows

$$A_{ij} = \int_{-t/2}^{t/2} \overline{Q}_{ij} dz \tag{2}$$

$$B_{ij} = \int_{-t/2}^{t/2} z \overline{Q}_{ij} dz \tag{3}$$

$$D_{ij} = \int_{-t/2}^{t/2} z^2 \overline{Q}_{ij} dz \tag{4}$$

where t is the laminate thickness and $\overline{Q}_{ij}$ are the transformed layer stiffness components. Inverting Eq. (1) results in the following

$$\left\{ \begin{array}{c} \varepsilon_x \\ \varepsilon_y \\ \gamma_{xy} \\ \kappa_x \\ \kappa_y \\ \kappa_{xy} \end{array} \right\} = \left[\begin{array}{cccccc} a_{11} & a_{12} & a_{16} & b_{11} & b_{12} & b_{16} \\ a_{21} & a_{22} & a_{26} & b_{21} & b_{22} & b_{26} \\ a_{61} & a_{62} & a_{66} & b_{61} & b_{62} & b_{66} \\ b_{11} & b_{21} & b_{61} & d_{11} & d_{12} & d_{16} \\ b_{12} & b_{22} & b_{62} & d_{21} & d_{22} & d_{26} \\ b_{16} & b_{26} & b_{66} & d_{61} & d_{62} & d_{66} \end{array} \right] \left\{ \begin{array}{c} N_x \\ N_y \\ N_{xy} \\ M_x \\ M_y \\ M_{xy} \end{array} \right\} \tag{5}$$

The effective longitudinal elasticity modulus E_{eff} can be calculated from Eq. (5) as

$$E_{eff} = \frac{1}{a_{11}t} \tag{6}$$

In some of the references (Polyzois *et al.* 1998, Raftoyiannis and Polyzois 2007), an approximate equation is utilized (in the planned parametric study) instead of Eq. (6) for the effective modulus E_{eff}, which limits the good accuracy of the results to the laminates with the large number of layers (more than 20 layers). However, in the current study, Eq. (6), which is the precise equation of E_{eff} will be employed that provides accurate values for the effective modulus even for the laminates with few layers.

3. Finite element formulation

The general geometry of a tapered composite pole is shown in Fig. 1. In order to accurately approximate the vibration behavior of the tapered poles, tapered beam finite element (Polyzois *et al.* 1998) is utilized. The tapered beam of length L and circular hollow cross-section with uniform thickness t shown in Fig. 2 is considered. The radii at the small and the large ends are R_1 and R_2, respectively. Since the cross-section is thin-walled, the cross-sectional area and moment of inertia are computed as $A = 2\pi Rt$ and $I = \pi R^3 t$, where the radius R varies linearly over the length. This implies a linear variation of the area A and a cubic variation of the moment of inertia I with respect
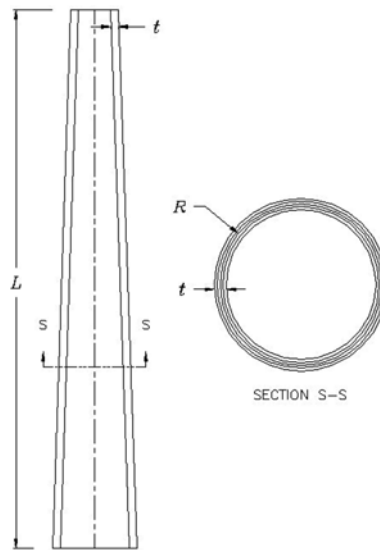

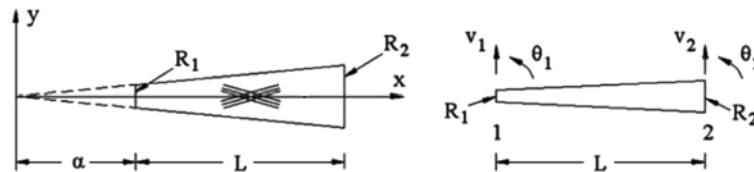Fig. 1 General geometry of a tapered composite pole

Fig. 2 Coordinate system and degrees of freedom of the tapered element (Polyzois *et al.* 1998)

to the length L. Thus, it is convenient to adopt a coordinate system x-y (Fig. 2), in which the area and moment of inertia are expressed as follows

$$A = A_0 x, \quad I = I_0 x^3 \tag{7}$$

Since $R_2/R_1 = (L + \alpha)/\alpha$, the shift α with respect to the coordinate origin is defined geometrically by

$$\alpha = \frac{L}{R_2/R_1 - 1} \tag{8}$$

where, A_0 and I_0, are coefficients defined as follows

$$A_0 = 2\pi\left(\frac{R_1}{\alpha}\right)t; \quad I_0 = \pi\left(\frac{R_1}{\alpha}\right)^3 t \tag{9}$$

The equation of motion for flexural free vibrations of the tapered beam is (Rao 1995)

$$\rho A \frac{\partial^2 v}{\partial t^2} + \frac{\partial^2}{\partial x^2}\left(EI\frac{\partial^2 v}{\partial x^2}\right) = 0 \tag{10}$$

where ρ is the mass density of the composite material, and E is the effective longitudinal modulus. In view of Eq. (7), it is obtained

$$\rho A_0 x \frac{\partial^2 v}{\partial t^2} + \frac{\partial^2}{\partial x^2}\left(EI_0 x^3\frac{\partial^2 v}{\partial x^2}\right) = 0 \tag{11}$$

The shape functions required for the finite element procedure can be obtained by solving the following static equilibrium equation

$$\frac{\partial^2}{\partial x^2}\left(EI_0 x^3\frac{\partial^2 v}{\partial x^2}\right) = 0 \tag{12}$$

The general solution of the above equation is

$$v(x) = c_1 x + c_2 \ln x + c_3\frac{1}{x} + c_4 \tag{13}$$

or in a matrix form

$$v(x) = \left\{x \quad \ln x \quad \frac{1}{x} \quad 1\right\}\begin{Bmatrix} c_1 \\ c_2 \\ c_3 \\ c_4 \end{Bmatrix}_f = \mathbf{g}_f^T \mathbf{c}_f \tag{14}$$

where subscript f is related to flexure. The coefficients $c_{f,i}$ ($i = 1, 2, 3, 4$) are related to the nodal displacements as follows

$$\begin{Bmatrix} v_1 \\ \theta_1 \\ v_2 \\ \theta_2 \end{Bmatrix} = \begin{bmatrix} \alpha & \ln\alpha & \dfrac{1}{\alpha} & 1 \\ 1 & \dfrac{1}{\alpha} & -\dfrac{1}{\alpha^2} & 0 \\ \alpha+L & \ln(\alpha+L) & \dfrac{1}{\alpha+L} & 1 \\ 1 & \dfrac{1}{\alpha+L} & -\dfrac{1}{(\alpha+L)^2} & 0 \end{bmatrix} \begin{Bmatrix} c_1 \\ c_2 \\ c_3 \\ c_4 \end{Bmatrix}_f \tag{15a}$$

or in a concise form

$$\mathbf{v} = \mathbf{N}_f \mathbf{c}_f \tag{15b}$$

Inverting Eqs. (15a) and (15b) and using Eq. (14), the deflection $v(x)$ are related to the nodal displacements as follows

$$v(x) = \mathbf{g}_f^T \mathbf{N}_f^{-1} \mathbf{v} = \mathbf{g}_f^T \mathbf{B}_f \mathbf{v} \tag{16}$$

From Eq. (16) it is found that

$$\mathbf{v}'' = \mathbf{g}_f''^T \mathbf{c}_f = \mathbf{g}_f''^T \mathbf{B}_f \mathbf{v} \tag{17}$$

where

$$\mathbf{g}_f''^T = \left\{ 0 \quad -\dfrac{1}{x^2} \quad \dfrac{2}{x^3} \quad 0 \right\} \tag{18}$$

The strain energy W of the element is

$$W = \frac{1}{2}\int_\alpha^{\alpha+L} EI\left(\frac{\partial^2 v}{\partial x^2}\right)^2 dx = \frac{1}{2}\mathbf{v}^T \mathbf{B}_f^T [\int_\alpha^{\alpha+L} \mathbf{g}_f''(EI_0 x^3)\mathbf{g}_f''^T dx] \mathbf{B}_f \mathbf{v} \tag{19}$$

Thus, the element stiffness matrix $\mathbf{K}_f$ is

$$\mathbf{K}_f = \mathbf{B}_f^T [\int_\alpha^{\alpha+L} \mathbf{g}_f''(EI_0 x^3)\mathbf{g}_f''^T dx] \mathbf{B}_f = \mathbf{B}_f^T \mathbf{k}_f \mathbf{B}_f \tag{20}$$

where $\mathbf{k}_f$ is

$$\mathbf{k}_f = EI_0 \begin{bmatrix} 0 & 0 & 0 & 0 \\ 0 & \ln(\alpha+L)-\ln\alpha & \dfrac{2}{\alpha+L}-\dfrac{2}{\alpha} & 0 \\ 0 & \dfrac{2}{\alpha+L}-\dfrac{2}{\alpha} & \dfrac{2}{\alpha^2}-\dfrac{2}{(\alpha+L)^2} & 0 \\ 0 & 0 & 0 & 0 \end{bmatrix} \tag{21}$$

The kinetic energy T of the element is

$$T = \frac{1}{2}\int_{\alpha}^{\alpha+L} \rho A\left(\frac{\partial v}{\partial t}\right)^2 dx = \frac{1}{2}\dot{\mathbf{v}}^T \mathbf{B}_f^T [\int_{\alpha}^{\alpha+L} \mathbf{g}_f(\rho A_0 x)\mathbf{g}_f^T dx]\mathbf{B}_f \dot{\mathbf{v}} \tag{22}$$

and the element mass matrix $\mathbf{M}_f$ is

$$\mathbf{M}_f = \mathbf{B}_f^T [\int_{\alpha}^{\alpha+L} \mathbf{g}_f(\rho A_0 x)\mathbf{g}_f^T dx]\mathbf{B}_f = \mathbf{B}_f^T \mathbf{m}_f \mathbf{B}_f \tag{23}$$

where the terms of $\mathbf{m}_f$ are given in explicit form as

$$m_{f,11} = \frac{1}{4}\rho A_0\{(\alpha+L)^4 - \alpha^4\} \tag{24a}$$

$$m_{f,12} = \frac{1}{9}\rho A_0\{(\alpha+L)^3(3\ln(\alpha+L)-1) - \alpha^3(3\ln\alpha-1)\} \tag{24b}$$

$$m_{f,13} = \frac{1}{2}\rho A_0\{(\alpha+L)^2 - \alpha^2\} \tag{24c}$$

$$m_{f,14} = \frac{1}{3}\rho A_0\{(\alpha+L)^3 - \alpha^3\} \tag{24d}$$

$$m_{f,22} = \frac{1}{4}\rho A_0\{(\alpha+L)^2(2\ln^2(\alpha+L)-2\ln(\alpha+L)+1) - \alpha^2(2\ln^2\alpha-2\ln\alpha+1)\} \tag{24e}$$

$$m_{f,23} = \rho A_0\{(\alpha+L)(\ln(\alpha+L)-1) - \alpha(\ln\alpha-1)\} \tag{24f}$$

$$m_{f,24} = \frac{1}{4}\rho A_0\{(\alpha+L)^2(2\ln(\alpha+L)-1) - \alpha^2(2\ln\alpha-1)\} \tag{24g}$$

$$m_{f,33} = \rho A_0\{\ln(\alpha+L) - \ln\alpha\} \tag{24h}$$

$$m_{f,34} = \rho A_0 L \tag{24i}$$

$$m_{f,44} = \frac{1}{2}\rho A_0\{(\alpha+L)^2 - \alpha^2\} \tag{24j}$$

Thus, the equilibrium equation for the tapered beam element in flexural mode (neglecting the damping effect) can be written in the matrix form as follows

$$\mathbf{M}_f\ddot{\underline{\delta}} + \mathbf{K}_f\underline{\delta} = \underline{\mathbf{Q}} \tag{25}$$

where $\underline{\delta}$ is the nodal displacement vector and $\mathbf{Q}$ is the nodal force vector.

In the case of symmetric laminate, all the B_{ij} terms, and in the case of anti-symmetric one, all the B_{ij} terms except B_{16} and B_{26}, are equal to zero. Hence, for these two types of laminates, bending-extension coupling vanishes (it is an approximate for anti-symmetric laminate) and axial vibration of the FRP pole is uncoupled from flexural vibration. Since flexural vibration of transmission poles is more important, in the present numerical investigation of the free vibration, considering the symmetric or anti-symmetric laminates, flexural free vibration is only evaluated. Thus, the nodal displacement vector of the tapered element in flexural mode is

$$\underline{\delta} = \begin{Bmatrix} v_1 \\ \theta_1 \\ v_2 \\ \theta_2 \end{Bmatrix} \tag{26}$$

4. Flexible joint modeling

In order to ease in manufacturing, transportation and installation, long transmission poles are produced modular and then are connected together. The joint type among the parts of the long poles can be adhesive, or by screw or a combination of mechanical and adhesive bonds. In the current research, a joint technique developed at the University of Manitoba of Canada (Raftoyiannis and Polyzois 2007) has been considered which is constructed by connecting two tapered cylindrical parts, utilizing an overlapping part of the jointed elements with length l, as shown in Fig. 3. A thin film with the thickness of t_j of resin (West System Epoxy 105 with hardener 206, in the mentioned case) is applied to the interface which after curing, acts as a glue to hold the two parts together. All member forces are transferred through the joint in the form of shear stresses τ, acting on the connection surfaces. In order to model the bending stiffness of the joint, a basic kinematic relation between shear strains γ of the interface resin and the joint rotation β is given by
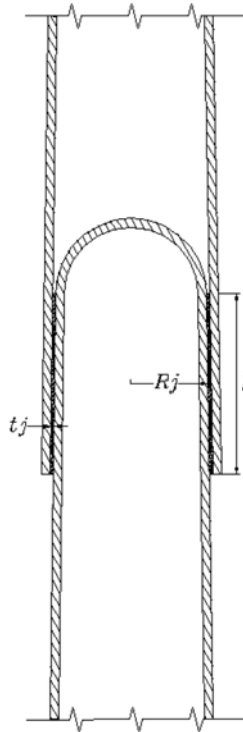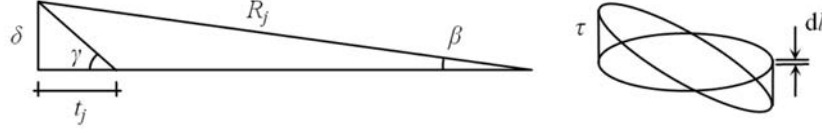

Fig. 3 The joint geometry

Fig. 4 Joint kinematics and shear stress distribution due to bending

$$\delta = t_j \gamma = R_j \beta \tag{27}$$

R_j is the radius of the interface at the joint position, which is shown in Fig. 4. The infinitesimal force dF due to shear stresses in the adhesive joint from the bending of the pole that acts on the joint circumference, is

$$dF = \tau l R_j \cos \varphi d\varphi \tag{28}$$

and since the moment arm is $R_j \cos \varphi$, the corresponding moment dM is

$$dM = R_j \cos \varphi dF = \tau l R_j^2 \cos^2 \varphi d\varphi \tag{29}$$

Introducing Eq. (28) as well as the well-known stress–strain relation $\tau = G\gamma$ (with G being the shear modulus of the applied resin) into Eq. (29) and integrating over the circumference, gives the following equation

$$M = \left(\int_0^{2\pi} G \frac{R_j}{t_j} l R_j^2 \cos^2 \varphi d\varphi \right) \beta \tag{30}$$

Considering the joint as a rotational spring, the term in the parenthesis is the spring constant c_f, corresponding to the bending stiffness of the joint, that is

$$c_f = G \frac{\pi R_j^3}{t_j} l \tag{31}$$

Finally, the dimensionless rotational spring stiffness C_f, is introduced as following

$$C_f = \frac{c_f}{\dfrac{E_{eff} \pi R_j^3 t}{L/2}} \tag{32}$$

where the denominator in Eq. (32) corresponds to the mean bending stiffness of both segments at the joint position.

5. Numerical results and discussion

In order to investigate the effect of various parameters on the vibration behavior of composite poles, based on the tapered beam finite element model, a computer code is provided by MATLAB 7.1 software to perform modal analysis of the FRP poles. At first, to study the convergence of the mentioned code, the fundamental natural frequency of a typical pole named as pole "A" with
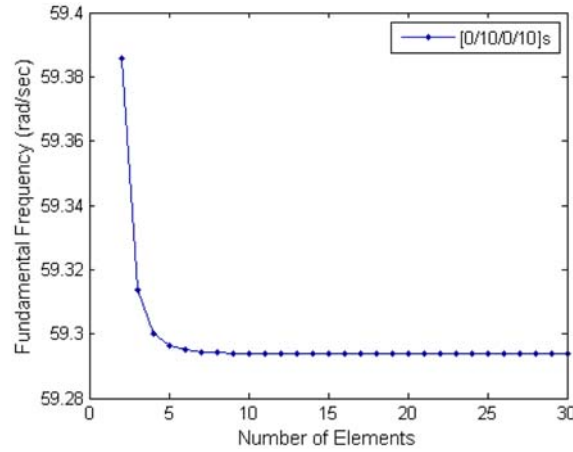
Fig. 5 Convergence study for the tapered beam element model, for the pole "A" with $[0/10/0/10]_s$ lay-up

Table 1 Geometric characteristics of the pole "A"

Length, L (mm)	Top diameter, d_1 (mm)	Bottom diameter, d_2 (mm)	Wall thickness, t (mm)	Number of laminae
4000	72	144	4	8

Table 2 Properties of E-glass/polyester unidirectional lamina with fibre volume fraction $V_f = 0.65$ (Polyzois *et al.* 1998)

Longitudinal modulus, E_L (GPa)	Transverse modulus, E_T (GPa)	Shear modulus, G_{LT} (GPa)	Major Poisson's ratio, ν_{LT}	Density, ρ (kg/m^3)
48	13.30	5.17	0.235	1904

geometric characteristics in Table 1, made from E-glass/polyester with fibre volume fraction of 0.65 (the material properties are given in Table 2), and $[0/10/0/10]_s$ lay-up with respect to the pole axis, is plotted against the number of elements in Fig. 5. In Table 2, E_L is the longitudinal elasticity modulus; E_T, the transverse elasticity modulus; ν_{LT}, the major Poisson's ratio; and G_{LT}, the shear modulus of the lamina. As it is seen in Fig. 5, the tapered beam model has a rapid convergence since, if the number of elements is more than 5, the fundamental frequency becomes constant and is equal to 59.29 rad/sec. For validating the present model, a cylindrical FRP pole with mean diameter of 144 mm and other characteristics available in Table 1 and Table 2, having $[0/10/0/10]_s$ lay-up is considered. The fundamental frequency of flexural vibration of the cantilever pole ω_1, is obtained using the beam theory as following (Thomsen 2003)

$$\omega_1 = \frac{1.875^2}{L_p^2} \sqrt{\frac{E_{11}I}{\rho A}}$$
(33)

where E_{11} is the effective longitudinal modulus of the laminate, L_p is the pole length, ρ is the mass density, A and I are the cross-sectional area and moment of inertia, respectively. The fundamental frequency of the cylindrical pole using the present finite element model by 6 elements is obtained
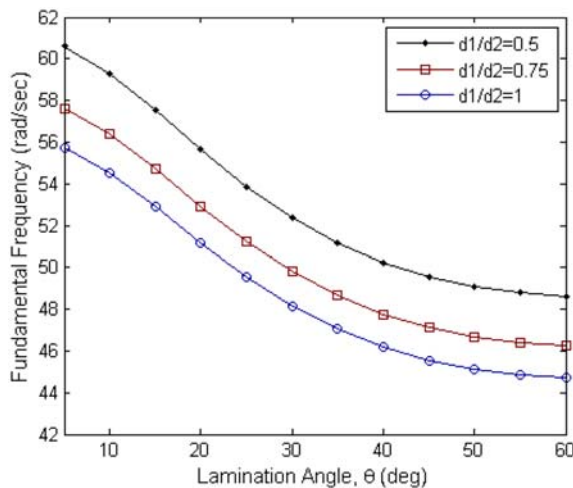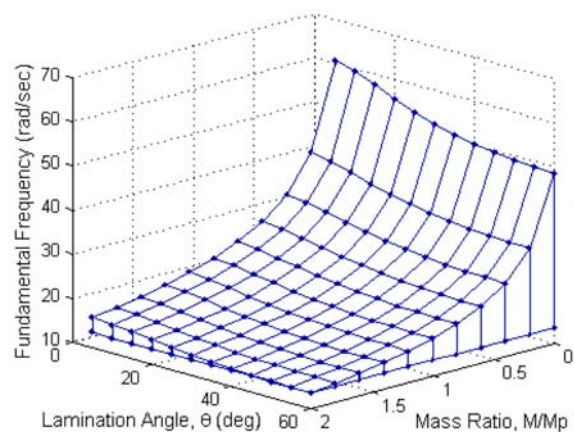
Table 3 Comparison of the natural frequencies of the pole "A" with [0/10/0/10]$_s$ lay-up, between the present and ANSYS models

Mode no.	Present model (rad/s)	ANSYS (rad/s)	Discrepancy (%)
1	59.29	59.12	0.3
2	284.05	277.31	2
3	733.15	692.53	5.8
4	1404.09	1270.0	10

54.522 rad/sec which has only a discrepancy of 0.01% with respect to the obtained quantity from Eq. (33) that is 54.515 rad/sec. Furthermore, a comparison with experimental results of the work by Caracoglia and Velazquez (2008) is presented. The first and second natural frequencies of a 12.8 m GFRP pole named "specimen B" (with the wall thickness of 6 mm and the concentrated mass of 36 kg at the top) are 0.63 and 4.98 Hz (3.96 and 31.29 rad/sec) respectively (Caracoglia and Velazquez 2008), in comparison with 0.76 and 4.98 Hz (4.77 and 31.29 rad/sec) obtained from the present finite element approach.

In the next step, pole "A" with [0/10/0/10]$_s$ lay-up is analyzed with total number of 2000 elements of type SHELL99 using ANSYS 11.0 commercial finite element software (ANSYS 2007). The first four natural frequencies obtained from the ANSYS code (flexural modes) and the present model, are compared together in Table 3. The maximum discrepancy with respect to the ANSYS results is for the fourth frequency and is equal to 9% which is acceptable. The obtained natural frequencies in this paper are more precise than those obtained in the references (Polyzois *et al.* 1998, Raftoyiannis and Polyzois 2007). Because, as mentioned before, in the present study the actual effective modulus of the laminate is utilized instead of the approximate expression used by others for the modulus.

The fundamental natural frequencies of the pole "A" with [0/θ/0/θ]$_s$ lay-up, for the various lamination angles θ, and the taper ratios d_1/d_2 (the pole base diameter d_2 is kept constant) is

Fig. 6 Fundamental frequency of the pole "A" with [0/θ/0/θ]$_s$ lay-up, for various taper ratios and lamination angles

Fig. 7 Fundamental frequency of the pole "A" with [0/θ/0/θ]$_s$ lay-up, for various mass ratios and lamination angles

illustrated in Fig. 6. It is observed that the lower d_1/d_2 ratio, the higher the fundamental frequency. In addition, the fundamental frequency is directly proportional to the effective modulus E_{eff} and hence, there is a significant drop of the natural frequency for the lamination angles greater than $\theta = 10^\circ$. A significant parameter that affects the dynamic behavior of transmission poles is the presence of a cross-arm that is installed at the top of the pole to hold the wires as well as possible transformer equipments. These devices are modeled in the present work as a concentrated mass M placed at the free end of the pole. To investigate the effect of the concentrated mass M at the pole tip, the fundamental frequency of the pole "A" with $[0/\theta/0/\theta]_s$ symmetric lay-up, is computed for the various cases of the lamination angle θ and the ratio M/M_p (M_p is the pole mass and for the pole "A" is equal to 10.34 kg), and the results are shown in Fig. 7. As it is observed, the higher the concentrated mass attached at the pole tip, the lower the fundamental frequency. Also, the fundamental frequency in the presence of the mass M is still directly proportional to the effective modulus of the pole (i.e., the fibre orientation in the laminate), but is greater for the smaller values of M/M_p ratios.

   In the next step of the analysis, the influence of the joint flexibility on the modular pole dynamic behavior is evaluated. For this purpose, another typical pole named as pole "B" which contains a flexible joint at the half of its length, with geometric characteristics in Table 4, $[(-10/10)_2]$ lay-up and the joint characteristics in Table 5, is considered. To ensure the accuracy of the results by the present code, the jointed pole with the total length of 5795 mm is also analyzed by ANSYS 11.0 software. In the ANSYS model, each part of the pole is discretized by the total number of 2000 elements of the type SHELL99 and the joint adhesive region by 400 elements of the type SOLID95. Surface-to-surface contact from bonded type is defined in the software between the adhesive outer surface and the pole inner surface for the upper part, and also between the adhesive inner surface and the pole outer surface for the lower part, using CONTACT174 and TARGET170 elements (ANSYS 2007) (Fig. 8). Then, a cohesive zone material model is added to the contact elements' material properties which has only provided from this version of ANSYS software. The first four natural frequencies of the flexural free vibration of the jointed pole "B" by both ANSYS and the

Table 4 Geometric characteristics of the jointed pole "B"

Length of each part (mm)	Material type	Tapered angle of each part	Tip diameter of top part, d_1 (mm)	Base diameter of bottom part, d_2 (mm)	Wall thickness, t (mm)	Number of laminae
3050	E-glass/polyester (with fibre volume fraction=0.65)	0.477°	119	210	2.4	4

Table 5 Joint characteristics

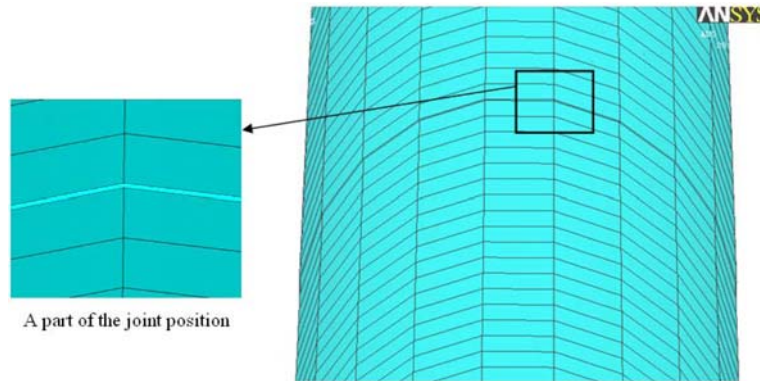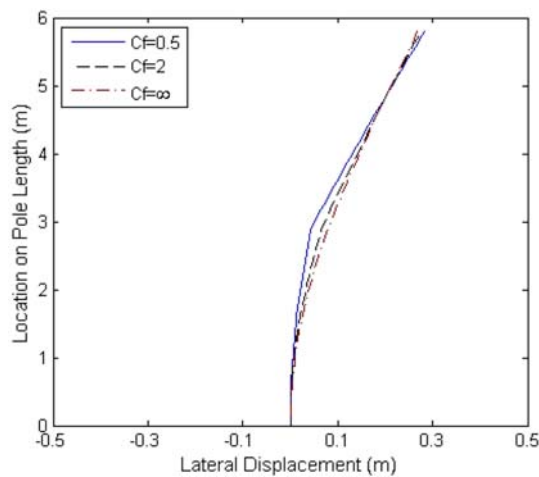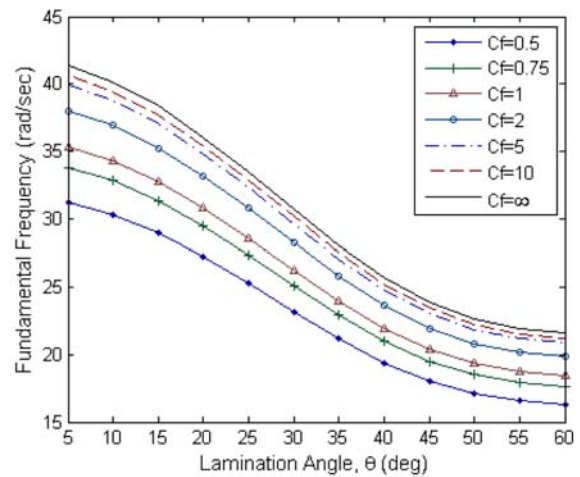| Adhesive (Raftoyiannis and Polyzois 2007): West System Epoxy 105 with hardener 206				Adhesive thickness, t_j (mm)	Joint length (mm)
Elasticity modulus (GPa)	Tensile strength (MPa)	Poisson's ratio	Density (kg/m³)		
3.172	50.47	0.3	1180	0.45	305

Fig. 8 Joint region of the jointed pole "B" for ANSYS model

Table 6 Comparison of the natural frequencies of the pole "B" with $[(-10/10)_2]_s$ lay-up, between the present and ANSYS models

Mode no.	Present model (rad/s)	ANSYS (rad/s)	Discrepancy (%)
1	40.15	40.40	-0.6
2	201.22	195.55	2.8
3	526.87	511.35	3
4	1013.65	917.60	10

Fig. 9 First mode shape of the jointed pole "B" with $[(-10/10)_2]$ lay-up, for various joint stiffnesses

Fig. 10 Fundamental frequency of the jointed pole "B" with $[(-\theta/\theta)_2]$ lay-up, for various lamination angles and joint stiffnesses

tapered beam element models are obtained and listed in Table 6 for comparison. The maximum discrepancy between the results is around 10% which shows a good agreement.

In order to evaluate the influence of the joint stiffness on the mode shape of the pole flexural free

Table 7 Properties of Kevlar149/polyester and carbon/polyester unidirectional laminas with V_f = 0.65 (Springer and Kollar 2003)

FRP type	Longitudinal modulus, E_L (GPa)	Transverse modulus, E_T (GPa)	Shear modulus, G_{LT} (GPa)	Major Poisson's ratio, v_{LT}	Density, ρ (kg/m^3)
Kevlar149/polyester	113.05	15.67	6.03	0.32	1314
carbon/polyester	157.25	16.0	6.11	0.255	1483

Table 8 Comparison of the natural frequencies of the pole "A" with [0/10/0/10]$_s$ lay-up, for various laminates

Mode no.	E-glass/polyester (rad/s)	Hybrid laminate 1 (rad/s)	Hybrid laminate 2 (rad/s)
1	59.29	72.01	77.29
2	284.05	344.99	370.27
3	733.15	890.43	955.63
4	1404.09	1705.32	1830.25

vibration, the first mode shape of the pole "B" with [(−10/10)$_2$] lay-up is plotted for the various dimensionless flexural stiffnesses of joint in Fig. 9. It is observed that in the case of the jointed pole, the fundamental mode shape of the flexural vibration is significantly different than the one corresponding to the continuous system (C_f = ∞). At the joint position, the continuity of the mode shape function is broken and the slopes of the top and bottom parts are changed. However, the larger the joint stiffness, the lower the breaking and the slope changes. The fundamental frequencies of the jointed pole "B" with [(−θ/θ)$_2$] lay-up are computed for various fibre orientations and dimensionless joint stiffnesses C_f, and are plotted in Fig. 10. It can be concluded that for relatively weak joints (C_f ≤ 2), the natural frequency reduces significantly with respect to the continuous pole, while for relatively strong joints (C_f > 5), the reduction is insignificant. Moreover, as the lamination angle θ increases, the natural frequency of the system decreases, because of decreasing the effective modulus.

In order to investigate the composite pole performance in the case of utilizing stiffer fibres in different laminae (in free vibration), Kevlar149 and carbon fibres are considered. Material properties of unidirectional lamina from Kevlar149/polyester and carbon/polyester with the fibre volume percentage of 65% are brought in Table 7. The first four natural frequencies of the continuous pole "A" with [0/10/0/10]$_s$ symmetric lay-up, for the plain E-glass/polyester laminate and the hybrid laminates 1 and 2 (the hybrid laminate 1 contained Kevlar149 fibre, and the hybrid laminate 2 contained carbon fibre only at the inner and outer layers beside the other layers with E-glass fibre), are calculated and listed in Table 8. As it is expected, by utilizing stiffer fibres at the inner and outer layers of the FRP pole cross-section, the natural frequencies increase. For example, in the case of the typical pole "A", using Kevlar149 fibre at the inner and outer laminas (hybrid laminate 1), there will be an increase of 21.5% in the fundamental frequency, and using carbon fibre (hybrid laminate 2) there will be an increase of 30.4%, with respect to the plain E-glass/polyester laminate.

6. Conclusions

By employing the tapered beam finite element model, the modal analysis of tapered FRP transmission poles with and without flexible joint, having a thin-walled circular cross-section, with various characteristics was performed. Because in the present study, the actual effective modulus of the cross-section laminate was used instead of an approximate expression for the modulus, more precise results obtained in comparison with other similar works. Another advantage of this act is that, the provided code is also applicable for the case of small number of laminae while the previous works aren't capable to be used in such case. Comparing the tapered beam element results with the ANSYS results and an experimental work, indicated that even with small number of elements in meshing, the results of the tapered beam model are with high degree of accuracy. Performing a parametric study on the typical composite poles showed that the small lamination angle, to be more tapered, the smaller concentrated mass at the pole tip, and increasing the joint stiffness for the jointed poles, cause the natural frequencies to be higher. In addition, it was concluded that, using the stiffer fibres (e.g., carbon or Kevlar), only at the inner and outer layers of the cross-section of the pole, causes further increase in stiffness and higher natural frequencies of the composite poles.

References

ANSYS, Inc. (2007), *ANSYS User's Manual for Rev. 11.0*, ANSYS, USA.

Caracoglia, L. and Jones, N.P. (2007), "Numerical and experimental study of vibration mitigation for highway light poles", *Eng. Struct.*, **29**, 821-831.

Caracoglia, L. and Velazquez, A. (2008), "Experimental comparison of the dynamic performance for steel, aluminum and glass-fiber-reinforced-polymer light poles", *Eng. Struct.*, **30**, 1113-1123.

Gould, P.L. and Basu, P.K. (1977), "Geometric stiffness matrices for the finite element analysis of rotational shells", *J. Struct. Mech.*, **5**, 87-105.

Ibrahim, S. and Polyzois, D. (1999), "Ovalization analysis of fibre-reinforced poles", *Compos. Struct.*, **45**, 7-12.

Jones, R.M. (1998), *Mechanics of Composite Materials*, Scripta Book Co., Washington DC.

Kim, N.I., Shin, D.K. and Park, Y.S. (2010), "Coupled stability analysis of thin-walled composite beams with closed cross-section", *Thin Wall. Struct.*, **48**, 581-596.

Lin, Z.M. (1995), "Analysis of pole-type structures of fibre-reinforced plastics by finite element method", Ph.D. Thesis, University of Manitoba, Canada.

Mabie, H.H. and Rogers, C.B. (1972), "Transverse vibrations of double-tapered cantilever beams", *J. Acoust. Soc. Am.*, **51**, 1771-1774.

Mabie, H.H. and Rogers, C.B. (1974), "Transverse vibrations of double-tapered cantilever beams with end support and with end mass", *J. Acoust. Soc. Am.*, **55**, 986-989.

Metiche, S. and Masmoudi, R. (2007), "Full-scale flexural testing on fiber-reinforced polymer (FRP) poles", *Open Civ. Eng. J.*, **1**, 37-50.

Mohamed, H. and Masmoudi, R. (2009), "Design optimization of GFRP pole structures using finite element analysis", *Proceeding of the ACMA 2009 Conference*, Tampa, Florida, USA.

Navaratna, D.R., Pian, T.H.H. and Wittmer, E.A. (1968), "Stability analysis of shell of revolution by the finite element method", *AIAA J.*, **6**, 355-360.

Noor, A.K., Burton, W.S. and Peters, J.M. (1991), "Assessment of computational models for multilayered composite cylinders", *Int. J. Solids Struct.*, **27**, 1269-1286.

Polyzois, D., Raftoyiannis, I.G. and Ibrahim, S. (1998), "Finite elements method for the dynamic analysis of tapered composite poles", *Compos. Struct.*, **43**, 25-34.

Raftoyiannis, I.G. and Polyzois, D. (2007), "The effect of semi-rigid connections on the dynamic behavior of

tapered composite GFRP poles", *Compos. Struct.*, **81**(1), 70-79.

Rao, S.S. (1995), *Mechanical Vibrations*, Addison Wesley, MA.

Springer, G.S. and Kollar, L.P. (2003), *Mechanics of Composite Structures*, Cambridge University Press, New York.

Thomsen, J.J. (2003), *Vibrations and Stability*, Springer Press, Berlin.

Yuan, R.L., Hasen, Z., Green, A. and Bisarnsin, T. (1991), "Fibre-reinforced plastic composite columns", *Proceedings of Specialty Conference on Advanced Composite Material in Civil Engineering Structures, ASCE,* 205-211.

Zabihollah, A. and Ganesan, R. (2010), "Buckling analysis of tapered composite beams using a higher order finite element formulation", *J. Reinf. Plast. Comp.*, **29**, 2663-2683.